Int J Biometeorol
DOI 10.1007/s00484-013-0653-z

ORIGINAL PAPER

Penman-Monteith approaches for estimating crop evapotranspiration in screenhouses—a case study with table-grape

Moran Pirkner · Uri Dicken · Josef Tanny

Received: 14 June 2012 / Revised: 24 December 2012 / Accepted: 14 February 2013

Abstract In arid and semi-arid regions many crops are grown under screens or in screenhouses to protect them from excessive radiation, strong winds, hailstorms and insects, and to reduce crop water requirements. Screens modify the crop microclimate, which means that it is necessary to accurately estimate crop water use under screens in order to improve the irrigation management and thereby increase water-use efficiency. The goal of the present study was to develop a set of calibrated relationships between inside and outside climatic variables, which would enable growers to predict crop water use under screens, based on standard external meteorological measurements and evapotranspiration (ET) models. Experiments were carried out in the Jordan Valley region of eastern Israel in a table-grape vineyard that was covered with a transparent screen providing 10 % shading. An eddy covariance system was deployed in the middle of the vineyard and meteorological variables were measured inside and outside the screenhouse. Two ET models were evaluated: a classical Penman-Monteith model (PM) and a Penman-Monteith model modified for screenhouse conditions by the inclusion of an additional boundary-layer resistance (PMsc). Energy-balance closure analysis, presented as a linear relation between half-hourly values of available and consumed energy (1,344 data points), yielded the regression Y=1.05X–9.93 (W m^{-2}), in which Y = sum of latent and sensible heat fluxes, and X = net radiation minus soil heat flux, with R^2=0.81. To compensate for overestimation of the eddy fluxes, ET was corrected by forcing the energy balance closure. Average daily ET under the screen was 5.4±0.54 mm day^{-1}, in general agreement with the model estimates and the applied irrigation. The results showed that measured ET under the screen was, on average, 34 % lower than that estimated outside, indicating significant potential water saving through screening irrigated vineyards. The PM model was somewhat more accurate than the PMsc for estimating ET under the screen. A model sensitivity analysis illustrates how changes in certain climatic conditions or screen properties would affect evapotranspiration.

Keywords Energy balance · Penman-Monteith · Eddy covariance · Net radiation · Wind · Temperature

M. Pirkner · U. Dicken · J. Tanny (✉)
Institute of Soil, Water and Environmental Sciences,
Agricultural Research Organization, Volcani Center,
POB 6, Bet Dagan 50250, Israel
e-mail: tanai@volcani.agri.gov.il

List of symbols and abbreviations

Symbol	
B	Bowen ratio (−)
C_p	Specific heat of air (J kg^{-1} K^{-1})
D	Mean leaf diameter (m)
d	Canopy zero-plane displacement (m)
d_s	Screenhouse zero-plane displacement (m)
e_s,e_a	Saturated and actual vapour pressure, respectively (kPa)
G	Soil heat flux density (W m^{-2})
$G_{l,max}$	Maximum leaf resistance (s m^{-1})
G_s	Stomatal resistance (μmol s^{-1} m^{-2})
H_s	Screenhouse height (m)
H	Canopy sensible heat flux (W m^{-2})
H_f	Forced sensible heat flux (W m^{-2})
h	Canopy height (m)
LE	Canopy latent heat flux (W m^{-2})
LE_f	Forced latent heat flux (W m^{-2})
R	Gas constant, 8.3144 (J K^{-1} mol^{-1})
R_G	Global radiation (W m^{-2})
R_N	Net radiation (W m^{-2})
r_a	Aerodynamic resistance (s m^{-1})
r_b	Boundary layer resistance (s m^{-1})
r_c	Canopy resistance (s m^{-1})
r_l	Leaf resistance (s m^{-1})

Published online: 10 April 2013

S	Sensitivity coefficient (−)
$S_{photons}$	Regression constant (μmol s^{-1} m^{-2})
T_a	Air temperature (°C)
T_l	Leaf temperature (K)
u	Horizontal wind speed (m s^{-1})
z_m, z_h	Height of wind and humidity measurements (m)
z_{0m}	Roughness length for momentum (m)
z_{0h}	Roughness length for heat and water-vapour transfer (m)

Greek letters

α	Grass albedo = 0.23 (−)
Δ	Slope of saturation vapour pressure- temperature curve (kPa $°C^{-1}$)
Δ^*	$=\Delta\ (1 + r_b/r_a)$
γ	Psychrometric constant (kPa K^{-1})
γ^*	$=\gamma(1+(r_c + r_b)/r_a)$
ν	Air kinematic viscosity (m^2 s^{-1})
ρ_a	Air density (kg m^{-3})

Abbreviations

EC	Eddy covariance
ET	Evapotranspiration
LAI	Leaf area index
NSE	Nash-Sutcliffe efficiency coefficient (−)
PAR	Photosynthetically active radiation (μmol s^{-1} m^{-2})
PM_{in}	Penman-Monteith model inside screenhouse
PM_{out}	Penman-Monteith model outside screenhouse
PMsc	Penman-Monteith model modified for screenhouse conditions
Press	Atmospheric pressure (Pa)
Re	Reynolds number (−)
RMSE	Root-mean-square error (units depend on the parameter)
VPD	Vapor-pressure deficit (kPa)
WI	Willmott index (−)

Subscripts

in out	Inside and outside the screenhouse respectively
m	Measured parameter
p	Predicted parameter

Introduction

In arid and semi-arid regions many crops are grown under screens to protect them from excessive radiation and consequent sunburn, to protect them from insects (Rossel and Ferguson 1979) and hail storms, and to prevent physical damage by strong winds (Tanny et al. 2006, 2010). The effects of screens on crop microclimate and water use have been investigated in several studies during the past two decades (Cohen et al. 2005; Desmarais et al. 1999; Dicken et al. 2012; Kittas et al. 2012; Möller et al. 2004; Moratiel and Martinez-Cob 2012; Rana et al. 2004; Raveh et al. 2003; Tanny and Cohen 2003; Tanny et al. 2003, 2006, 2010; Teitel et al. 1996; Teitel and Wenger 2010). The screens not only reduce the wind speed near the crop but also modify the turbulence characteristics (Tanny and Cohen 2003; Siqueira et al. 2012) and thereby impair the contribution of the wind to heat- and water-vapor-exchange between the plants and the atmosphere. Siqueira et al. (2012) used a theoretical model to show that this effect reduced evapotranspiration in a shaded banana plantation, and also that the screen increased the air temperature and humidity near the canopy.

A screen cover or a screenhouse reduces the exchange rates of radiation, momentum and mass between the crop and atmosphere and, therefore, it could affect the plantation management. Thus, investigating the energy and mass fluxes and the associated microclimate in covered plantations is of significant interest from both scientific and practical viewpoints (Tanny and Cohen 2003; Tanny et al. 2003, 2006, 2009, 2010; Möller et al. 2004, 2010).

Recent studies (Tanny et al. 2006, 2010; Dicken et al. 2012) examined and demonstrated the suitability of the eddy covariance (EC) technique to directly measure evapotranspiration and CO_2 fluxes in large screenhouses. Results were promising: good closure of the energy balance, usually larger than 80 %, was achieved, and measured daily evapotranspiration values were consistent with the irrigation amounts applied by the grower. Even though the EC system was deployed relatively close to the canopy top, the spectral energy density decayed with the frequency at a rate close to the power of −5/3, suggesting that turbulence properties resembled the flow in the inertial sub-range of steady boundary layers.

Tanny et al. (2010) measured turbulent fluxes with two EC systems installed at two heights above the crop within a large banana screenhouse, and operated simultaneously. Similar friction velocities were measured at the two levels, validating the assumption of a constant-flux layer within the air gap between the canopy top and the horizontal screen. By examining integral turbulence characteristics, according to Foken et al. (2004), Tanny et al. (2010) showed that turbulence was marginally developed within the screenhouse, and energy-balance closure was satisfactory at both levels considered. However, better closure was obtained for the EC system at the lower level, presumably because of insufficient fetch for the upper system.

Crop water requirement is affected most by atmospheric water demand, which integrates the effects of radiation, wind, temperature and humidity, on crop microclimate. Hence, the modified microclimate under the screen, and especially the reduced radiation and wind speed, might reduce crop evapotranspiration (ET) (Rana et al. 2004; Moratiel and Martinez-Cob 2012). Although crop water requirements in open conditions are well documented in the

literature (e.g., Allen et al. 1998), their modification by screens has been much less studied. Therefore, tools that can estimate crop water use accurately in order to improve irrigation management and increase water-use efficiency in such protected environments are needed.

Table grapevine is an important crop in the Jordan Valley region of eastern Israel. Many growers in this region are making extensive use of shading screenhouses to protect the grapevines from excessive radiation and strong winds, which is allowing them to have more profitable productions (Y. Esquira, personal communication, 2012). The use of screens to cover grapevines is also common in other Mediterranean countries, like Spain (Moratiel and Martinez-Cob 2012) and Italy (Rana et al. 2004), where it was shown that evapotranspiration of covered vineyards was lower than that of exposed ones.

The general goal of the present study was to develop a simple method, based on standard external meteorological data and canopy properties, for predicting crop water requirements in a screenhouse. The model calculation used two approaches: the first was based on internal meteorological and canopy variables measured directly inside the screenhouse; the second was based on measured external meteorological variables and a set of calibration equations that relates them to corresponding internal variables. The second approach would be more feasible for growers because external meteorological variables are more attainable than internal ones. Two ET models were examined: a classical Penman-Monteith model (PM) and a PM model modified for screenhouse conditions by the inclusion of an additional boundary layer resistance (PMsc) (Möller et al. 2004).

Materials and methods

The field experiment

Measurements were conducted in a flat-roof screenhouse at Kibbutz Beqaot in the Jordan Valley of eastern Israel (33°06′N; 35°30′E; 280 m below mean sea level), in which a vineyard plantation was grown. The local summer climate is rainless and predominantly sunny with little variation from day to day. The transparent shading screen (Leno Crystal woven net; Polysack, Kibbutz Nir Yitzhak, Israel) was made of clear, round polyethylene monofilaments, 0.3 mm in diameter, and had rectangular holes measuring 2×3 mm. Nominal shading by this screen is 10 % (manufacturer's data). The screenhouse was rectangular, 240 m× 175 m in horizontal dimensions, 3.1 m high, with the longer side oriented west–east, which is the prevailing wind direction. Table grapevines (cultivar S.B.S.) were planted in the spring of 2008, with spacing of 3 m between rows and 1.5 m between plants in the row. Drip irrigation was applied according to standard recommendations for vineyards in the region and tensiometer readings. The water application rates ranged from 4.5 to 6 mm per day during the measurement period. The area surrounding the screenhouse was flat, and there were similar vineyard screenhouses to the west and north, a tomato greenhouse to the east, and an open field to the south. Results from 28 measurement days (non-consecutive) from 5 May to 6 June 2010, which represents the major irrigation period of the vineyard, are presented. During this period, the vineyard was mature and developed homogenously with a uniform plant height of 2.4 m and a constant leaf area index of 4.41 that was maintained by thinning.

An EC system was deployed at a height of 2.74 m on one of the screenhouse supporting poles near its center, which allowed a minimum fetch of about 87 m in all wind directions (Fig. 1). The system consisted of a three-axis ultrasonic anemometer (Model CSAT3; Campbell Scientific, Logan, UT) and an Infra Red Gas Analyzer (Model LI-7500; LI-COR, Lincoln, NE). The EC system was, at most, 1.24 m above plant zero-plane displacement, as estimated according to Stanhill (1969), and assuming neutral stability. Thus, with the minimum fetch of 87 m, the height/fetch ratio of the sensors was suitable for surface flux measurements (Hsieh et al. 2000; Schmid 1997).

Raw signals were sampled at 10 Hz, recorded and processed continuously on line, with averages and covariances stored every 30 min on a CR5000 data logger (Campbell Scientific). This sampling rate is suitable for reliable measurements of turbulent fluxes and other turbulence characteristics in screenhouses (Tanny et al. 2006, 2010). All 10-Hz raw data were later processed to calculate the turbulent fluxes by using the MATLAB software package (Mathworks, Natick, MA). Latent heat flux raw data were corrected for coordinate system rotation (Kowalski et al. 1996), sensor separation (Moore 1986), path averaging (Moore 1986) and density (Webb et al. 1980). Sensible heat

Fig. 1 The eddy covariance (EC) system deployed inside the screenhouse, under the screen and above the table-grape plants

flux raw data were corrected for coordinate system rotation and path averaging.

Additional measurements were taken to facilitate analysis of the energy-balance closure. Net radiation was measured with a net radiometer (Q*7.1; REBS, Bellevue, WA) installed at a height of 2.8 m on a pole 6 m south of the EC system. Internal dry- and wet-bulb temperatures were measured with four aspirated psychrometers mounted on the same pole, shielded from direct solar radiation, and positioned 0.5, 1.15, 1.9 and 2.7 m above the ground. Soil heat flux was measured with six soil heat-flux plates (HFT-3.1; REBS) installed at a depth of 0.08 m; three of them were installed in the wet soil between plants along the hedgerow, and three in the dry soil along the path between hedgerows. To calculate the change in soil heat storage, two thermocouples were installed in the soil layer above each plate at depths of 0.02 and 0.06 m. Soil heat flux and storage were measured as recommended by Campbell Scientific (1998) and were calculated by using soil water content and bulk density, as determined from local soil samples (after Tanny et al. 2006). Because of technical problems, these soil measurements were made only during 6 days (28 April–10 May 2010) before the main experiment period and were used to establish a relationship between soil heat flux and internal net radiation. This relationship was later used to estimate soil heat flux from measured internal net radiation during the main experiment. During these 6 days, soil and plant characteristics—e.g., irrigation, plant height, leaf area index (LAI)—were the same as during the main measurement period.

The same CR5000 data logger was used to record 30-min averages of the measured variables: net radiation, soil heat flux and temperatures, and mean wind components. The aspiration fans of the psychrometers were operated for the last 5 min, and dry- and wet-bulb temperatures were measured and averaged during the last minute of every 30-min interval. These data were also recorded on the CR5000 data logger. All the equipment was powered by car batteries that were charged during the day by solar panels that were mounted on the screen, about 18 m away from the measurement region.

Observations showed that only the soil near the irrigation drippers was wet. The area of wet soil surface was estimated by direct measurements on the 9-m^2 area around a block of three plants: the average of five replications gave the ratio of the average wet soil area to total soil area of the block, which was designated as the area fraction of wet soil, whose value was 0.33.

LAI was determined every 2 weeks as the mean leaf area of 50 leaves, as measured with a laboratory DELTA-T area-meter (DELTA-T Devices, Cambridge, UK), multiplied by the total leaf number per tree (counted in the field), and divided by ground area per tree.

Stomatal conductance (G_s) and leaf temperature (T_l) were measured with a Portable Photosynthesis System (CIRAS-2; PP Systems International, Amesbury, MA). Measurements were taken every 1.5 h from sunrise to sunset on 12 May 2010: at least three different whole green sunlit leaves, replicated on each of five different plants, were measured, and the measured G_s (μmol H_2O s^{-1} m^{-2}) was related to photosynthetically active radiation (PAR) by:

$$G_s = \frac{G_{l,\max}}{1 + \frac{S_{photons}}{PAR}} \tag{1}$$

by means of the Excel solver utility. The calculations yielded

$$G_{l,max} = 443.33(\mu\text{mol } H_2O \text{ s}^{-1} \text{ m}^{-2}) \text{ and}$$
$$S_{photons} = 585.18(\mu\text{mol s}^{-1} \text{ m}^{-2}),$$

in which PAR is the measured photosynthetically active radiation (μmol s^{-1} m^{-2}). Mean hourly measured T_l was related to air temperature by the linear regression:

$T_l(\text{K}) = 0.59T_a + 15.55 + 273.15\left(\text{R}^2 = 0.96\right)$ in which T_a is in °C.

Instruments for measuring external meteorological data were mounted on a tower about 500 m west of the screenhouse. Global radiation at a height of 6.4 m was measured with a CM-5 radiometer (Kipp and Zonen, Delft, the Netherlands); air temperature and relative humidity at a height of 8.2 m with a model HMP45C (Vaisala, Helsinki, Finland); and wind speed and azimuth at 10 m with a model 05103 anemometer (R. M. Young, Traverse City, MI). Actual sensor heights were included in the calculations of the resistances in the PM models as described below.

Evapotranspiration models

Two ET models were examined: a Penman-Monteith model for a vineyard crop inside (PM_{in}) and outside (PM_{out}) the screenhouse; and a Penman-Monteith model modified for screenhouse conditions (PMsc) by the inclusion of an additional boundary layer resistance. A general expression for these two models is:

$$ET = \frac{\Delta^*(R_N - G)}{\Delta^* + \gamma*} + \frac{\rho_a C_p (e_s - e_a)}{r_a(\Delta^* + \gamma^*)} \tag{2}$$

in which

$$\Delta^* = \Delta\left(1 + \frac{r_b}{r_a}\right) \quad \textit{and}$$
$$\gamma^* = \gamma\left(1 + \frac{r_c + r_b}{r_a}\right) \tag{3}$$

ET is the evapotranspiration (W m^{-2}), Δ is the slope of the saturation vapor pressure-temperature curve (kPa K^{-1}), R_N is the canopy net radiation (W m^{-2}), G is the soil heat-flux density (W m^{-2}), ρ_a is air density (kg m^{-3}), C_p is air

specific heat at constant pressure (J kg^{-1} K^{-1}), e_s and e_a are the saturated and actual vapor pressure (kPa), γ is the psychrometric constant (kPa K^{-1}), r_a is the aerodynamic resistance (s m^{-1}), r_b is the screenhouse boundary layer resistance (s m^{-1}) and r_c is the canopy resistance (s m^{-1}). The two models mentioned above—PM and PMsc—differ in the expressions for the resistances in Eqs. (2) and (3), as explained below. The various parameters of the two models are summarized in Table 1.

The PM model

For r_b=0, Δ* and γ* revert to their original values, Δ and $\gamma(1+r_c/r_a)$, respectively, and Eq. (2) represents the classical PM model (Allen et al. 1998). The aerodynamic resistance is calculated by:

$$r_a = \ln\left[\frac{z_m-d}{z_{0m}}\right]\ln\left[\frac{z_h-d}{z_{0h}}\right]k^{-2}u^{-1}$$
$$d = 10^{0.9793\log 100h-0.1536}/100 \quad (4)$$

in which d is the zero-plane displacement height (m) (Stanhill 1969), h is the canopy height (m), z_m and z_h are the heights at which wind and humidity, respectively, are measured, and z_{0m} and z_{0h} are the roughness lengths for momentum and for heat and water vapor transfer, calculated as 0.123 h and 0.0123 h, respectively.

The canopy resistance r_c is estimated from the stomatal resistance r_l as:

$$r_c = \frac{2r_l}{LAI}$$
$$r_l = \frac{\text{Press}}{(0.001G_sRT_l)}, \quad (5)$$

in which Press is the atmospheric pressure (Pa), G_s (μmol H_2O s^{-1} m^{-2}) is the stomatal conductance estimated from Eq. (1), R is the universal gas constant, 8.3144 (J K^{-1} mol^{-1}) and T_l (K) is leaf temperature calculated from air temperature.

The PMsc model

Equation (2), with $r_b \neq 0$ and r_a and r_c given by Eqs. (4) and (5), respectively, is the PMsc model (Möller et al. 2004), in which r_b represents the internal boundary layer resistance across the air layer between the top of the leaves and the level of the screenhouse zero plant displacement, estimated as $d_s=0.8H_s$ (Möller et al. 2004), where H_s is the screenhouse height. The value of r_b was calculated from heat transfer correlations (Holman 1989) that depend on the nature of the flow. To distinguish between laminar and turbulent flows, the leaf boundary layer Reynolds number was estimated as $\text{Re} = u_{in}D/\nu$, in which D is the mean leaf diameter, u_{in} is the internal air velocity and ν is the air kinematic viscosity. Under the screenhouse conditions of the present study the Reynolds number was always Re< 40,000, meaning that leaf boundary layers were always laminar (Grace 1980), so that:

$$r_b = 305\left(\frac{D}{u_{in}}\right)^{0.5}. \quad (7)$$

Model calibration and verification

The whole measurement period was divided into two equal periods: calibration (14 non-consecutive days, 5–20 May); and verification (14 non-consecutive days; 21 May–6 June). Data obtained during the calibration period were used to derive a set of regressions relating internal to external variables: internal temperature, wind speed and vapor-pressure deficit (VPD) were regressed against their corresponding external values; leaf stomatal resistance and internal net radiation were regressed against external global radiation.

During the verification period predicted values of the internal meteorological variables—R_N, T_a, VPD, wind speed and leaf resistance—were verified against the measured ones by linear regression. "Measured" leaf resistance was calculated from measured values of PAR and T_a by means of Eqs. (1) and (5). Soil heat flux was always estimated from measured net radiation as explained under "Energy balance and measured fluxes", below. During the verification period ET models were calculated twice: by using predicted inside data; and by using measured inside data. The calculated ET was verified against the directly measured ET.

Statistical analysis evaluated the agreement between models and measurements using RMSE, the Willmott index (WI) and the Nash-Sutcliffe efficiency (NSE) coefficient. The RMSE index range is: 0 < RMSE < ∞, with 0 being a perfect agreement. The ranges for the other two indexes are: 0 ≤ WI ≤1, −∞ < NSE ≤1, whereas for these indexes the value 1 represents a perfect agreement.

Table 1 Resistance equations and details of each model (PM_{in}, PM_{out} and PMsc) related to Eq. 2

Model	r_a (s m^{-1})	z_m, z_h, d (m)	r_b (s m^{-1})	r_c (s m^{-1})
PM_{in}	$r_a = \ln\left[\frac{z_m-d}{z_{0m}}\right]\ln\left[\frac{z_h-d}{z_{0h}}\right]k^{-2}u^{-1}$	2.7, 2.7, d	0	$\frac{2r_l}{LAI}$
PM_{out}	$r_a = \ln\left[\frac{z_m-d}{z_{0m}}\right]\ln\left[\frac{z_h-d}{z_{0h}}\right]k^{-2}u^{-1}$	10, 8.2, d	0	$\frac{2r_l}{LAI}$
PMsc	$r_a = \ln\left[\frac{z_m-d}{z_{0m}}\right]\ln\left[\frac{z_h-d}{z_{0h}}\right]k^{-2}u^{-1}$	10, 8.2, d_s	$305\left(\frac{D}{u_{in}}\right)^{0.5}$	$\frac{2r_l}{LAI}$

Sensitivity analysis

To generalize the results of this study for different climatic conditions or screen types, a model sensitivity analysis was carried out to show the model response to variations in the major meteorological variables. The sensitivity analysis was carried out in three phases, where each phase allows model sensitivity to be examined on a different level.

The first phase analyzed the sensitivity of each of the model variables, denoted as V, relative to a reference value, V_r, where all other model variables are kept constant in their reference value (Möller et al. 2004). In the second phase, the sensitivity coefficient of each variable, S_v, was calculated from the derivative $\partial ET/\partial V$. The sensitivity coefficients describe the rate of change of the model ET under the influence of a change of any parameter V. This calculation was performed numerically using differences between model and parameters values. In the third phase, and in order to simulate the behavior of the models under different climatic conditions, the sensitivity of the models to simultaneous changes in two variables was examined—one of the variables was one of the main meteorological parameters (VPD, T and R_N) and the other was wind speed.

Results

Energy balance and measured fluxes

The results of measurements taken during 6 days preceding the main experimental period were used to obtain a linear relationship between the measured soil heat flux (G) and the measured net radiation (R_N): $G = 0.19R_N - 23.18 \quad [Wm^{-2}]$ $(R^2 = 0.73; \quad N = 288)$. This equation was also used to estimate G_{in} and G_{out} during the calibration and verification periods, by using $R_{N\ in}$ and $R_{N\ out}$, respectively, where $R_{N\ out}$ was estimated according to Monteith and Unsworth (1990):

$$R_{N\,out} = (1-\alpha)R_{G\,out} - \left(107 - 0.3T_{a,out}\right) \quad (8)$$

in which α (= 0.23) is the albedo of grass.

Energy balance closure analysis (Fig. 2) appears to be divided into two regimes. For morning and afternoon hours (relatively low fluxes, R_N–$G \leq 340$) , the closure slope is 0.86 (R^2=0.80) lower than 1, indicating energy deficit, as is common in the literature (Wilson et al. 2002; Franssen et al. 2010). On the other hand, at midday hours (R_N–$G \geq 340$), energy excess was obtained. This non-linear behavior may be the result of advective effects associated with high wind speeds at midday hours. Nevertheless, the overall slope of the energy balance closure resulted in $LE + H = 1.05(R_N - G) - 9.93$ (R^2=0.81, 672 data points).

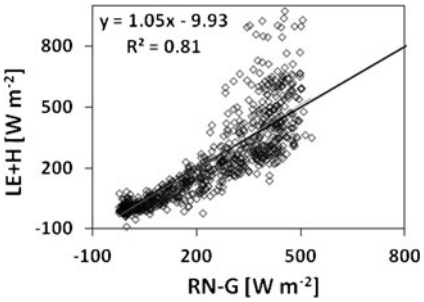

Fig. 2 Energy-balance closure before forcing: the relation between consumed energy ($LE + H$), as measured directly by the EC technique, and available energy ($R_N - G$) for 1,344 half-hourly data points

The Penman-Monteith models examined in this work are based on a perfect energy-balance closure, i.e., a unit slope and zero intercept of the preceding equation. Therefore, to establish a common basis for comparison of the ET values as estimated with the various evapotranspiration models, each half-hourly LE was forced to fit a perfect energy-balance closure (Twine et al. 2000). This modification was based on the assumption that, although measured sensible (H) and latent (LE) heat fluxes were generally overestimated (Fig. 2), the ratio between them, i.e., the Bowen ratio, $B = H/LE$, was measured correctly. By means of this procedure, a forced latent heat flux, LE_f was estimated for each half hour and, in turn, a forced sensible heat flux was calculated as the residual energy balance, $H_f = R_N - G - LE_f$. The diurnal variation curves of the four energy fluxes, after forcing the energy balance closure, are presented in Fig. 3.

Calibration and verification of model input data

Figure 4 presents the results of calibration and verification of the major model variables. All the variables inside the screenhouse were well correlated with corresponding external climatic variables during the 14 calibration days, with $R^2 \geq 0.88$ (Fig. 4a–e, left panels). As expected, the internal daytime

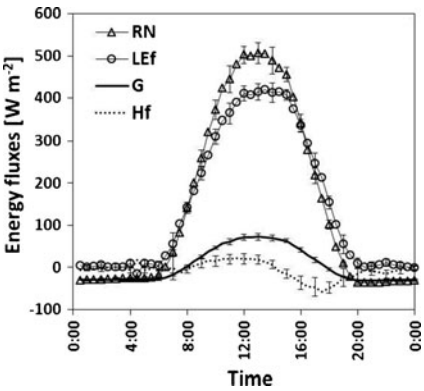

Fig. 3 Mean daily curves (28 days) of the energy fluxes. LE_f and H_f are latent and sensible heat fluxes, respectively, after forcing a perfect closure of the energy balance. *Vertical bars* 95 % confidence intervals

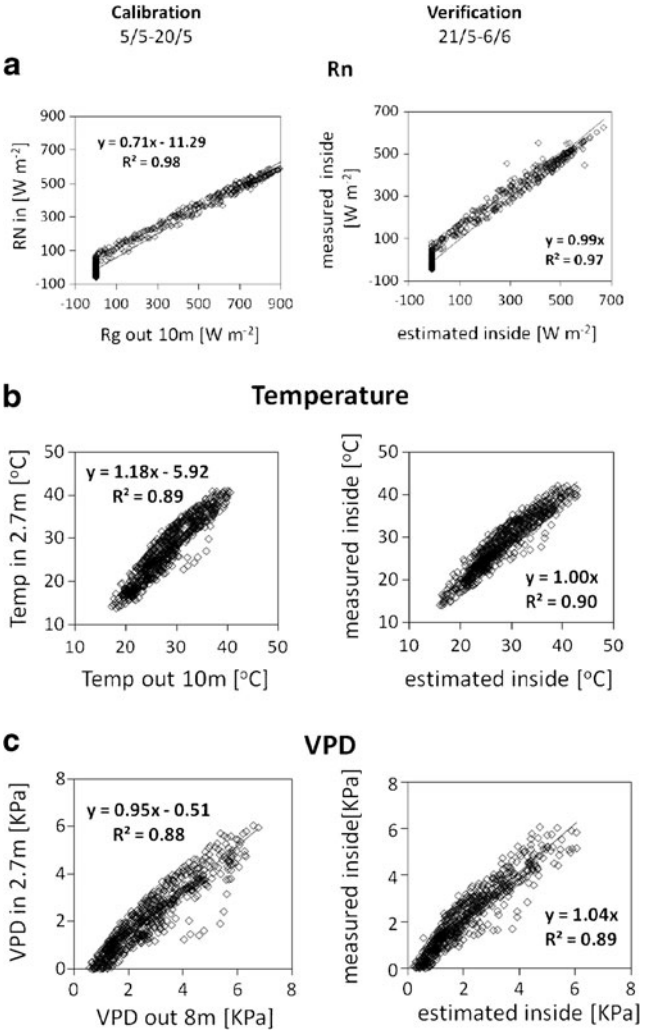

Fig. 4 Calibration (left-hand panels): dependence of the measured inside variables on external data during 14 days, and their regression equations. Verification (right-hand panels): linear regressions between the predicted values calculated with the calibration equations (from the left-hand panels) and the measured values during the 14 verification days. **a** Net radiation; **b** temperature; **c** vapor-pressure deficit (VPD); **d** wind speed; **e** leaf resistance

air temperature was somewhat higher than that outside, whereas the internal VPD and wind speed were lower than those outside. The following equations relate the inside and outside measured variables during the calibration period:

$$R_{N,in} = 0.71R_{G,out} - 11.29 \quad [W\ m^{-2}] \quad (R^2 = 0.98; \quad N = 672) \tag{9}$$

$$T_{a,in} = 1.18T_{a,out} - 5.92 \quad [^{\circ}C] \quad (R^2 = 0.89; \quad N = 672) \tag{10}$$

$$VPD_{in} = 0.95VPD_{out} - 0.51 \quad [kPa] \quad (R^2 = 0.88; \quad N = 672) \tag{11}$$

$$u_{in} = 0.19u_{out} - 0.13 \quad [m\ s^{-1}] \quad (R^2 = 0.86; \quad N = 672) \tag{12}$$

$$r_l = 5402.7R_{G,out}{}^{-0.56} \quad [s\ m^{-1}] \quad (R^2 = 0.95; \quad N = 348) \tag{13}$$

The predicted variables (identified by the subscript p) estimated by the above calibration equations of Fig. 4 (Eqs. 9–13) were well correlated with measured values during 14 days of verification, as shown in the right-hand panels of Fig. 4a–e. The linear regressions had slopes between 0.95 and 1.04, and R^2 values between 0.86 and 0.99. The verification relations are (Fig. 4, right-hand panels):

$$R_{N,m} = 0.99R_{N,p} \quad [Wm^{-2}] \quad (R^2 = 0.97; \quad N = 672) \tag{14}$$

$$T_{a,m} = 1.00T_{a,p} \quad [^{\circ}C] \quad (R^2 = 0.90; \quad N = 672) \tag{15}$$

$$VPD_m = 1.04VPD_p \quad [kPa] \quad (R^2 = 0.89; \quad N = 672) \tag{16}$$

$$u_m = 0.95u_p \quad [m\ s^{-1}] \quad (R^2 = 0.86; \quad N = 672) \tag{17}$$

$$r_{l,m} = 1.00r_{l,p} \quad [s\ m^{-1}] \quad (R^2 = 0.99; \quad N = 672) \tag{18}$$

Model estimations

Figure 5a, b illustrate the diurnal variation of the internal ET, as calculated by the two models, PM and PMsc, respectively, based on measured (subscript m) and predicted (subscript p) internal model variables, along with LE_f. Figure 5c, d depict the same data in scatter plots. Regressions between model and measured half hourly values were:

$$PM_m = 0.97LE_f + 9.52 \quad (R^2 = 0.99; \quad N = 48) \tag{19}$$

$$PM_p = 1.05LE_f - 10.99 \quad (R^2 = 0.99; \quad N = 48) \tag{20}$$

$$PMsc_m = 0.89LE_f + 12.73 \quad (R^2 = 0.99; \quad N = 48) \tag{21}$$

$$PMsc_p = 0.89LE_f + 12.72 \quad (R^2 = 0.99; \quad N = 48) \tag{22}$$

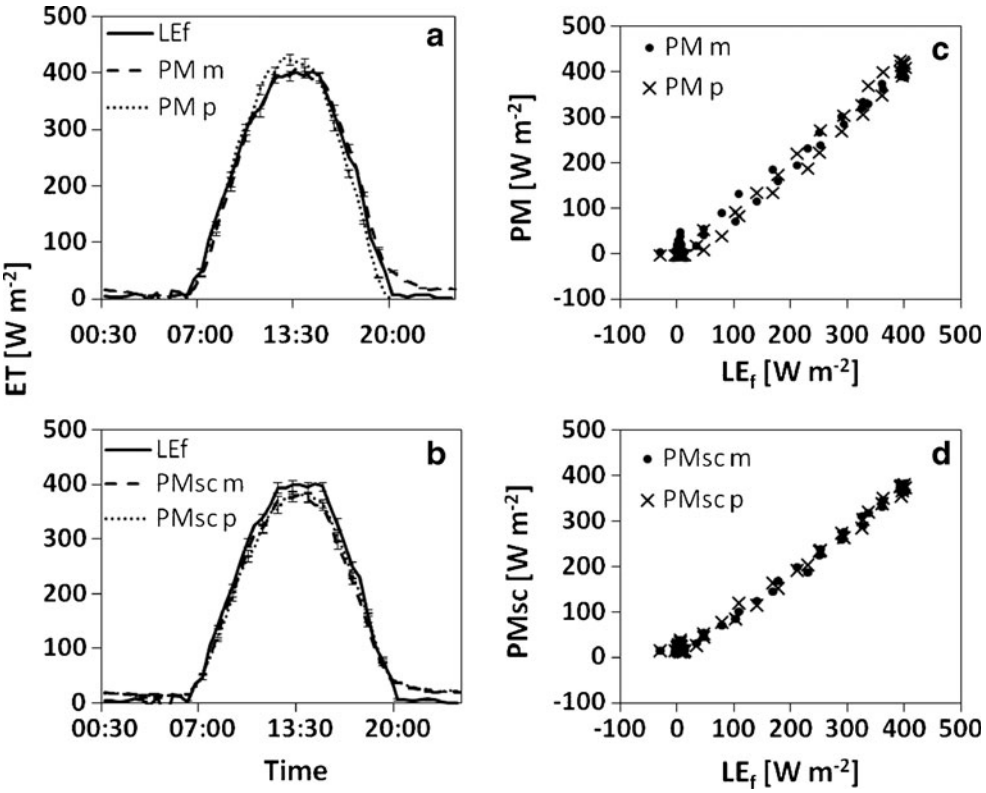

Fig. 5 **a**–**b** Average daily curves (14 days) of LE_f (*solid line*) and the two models. **a** Classic Penman-Monteith model (PM). **b** PM model modified for screenhouse conditions by the inclusion of an additional boundary-layer resistance (PMsc). Models were calculated from measured inside data (*dashed line*) and predicted inside data (*dotted line*) during the verification period. *Vertical bars* 95 % confidence intervals. Panels **c** and **d** depict the same data in scatter plots

Figure 6 presents the daily values of LE_f, part of the model predictions, and the irrigation applied by the grower: during the measurement period, LE_f was rather uniform with a daily average of 5.4±0.54 mm day^{-1}. Decreasing the irrigation from 6 mm day^{-1} to 4.5 mm day^{-1}, on 31 May did not greatly change LE_f, implying that soil water was available. Figure 6 clearly illustrates the effect of the screen in reducing the atmospheric water demand: during the verification period mean daily LE_f was 34 % lower than PM_{out}.

Table 2 presents the mean daily ratios between measured and modeled ET values for the calibration and verification periods. Rows I and II of Table 2 show these ratios based on models calculated from measured internal variables during calibration (row I) and verification (row II). The PM_{in} model yielded ET values equal to 97 and 102 % of LE_f, whereas the PMsc model predicted 92 and 96 % of LE_f, for the calibration and verification periods, respectively. The statistical measures show that during calibration PMin model performed better than PMsc, and vice-versa for the verification period.

When applied with predicted inside variables (Table 2, row III) the two models yielded results that were 4 % lower than LE_f and the statistical measures do not indicate a clear preference for any one of them. Comparing the performance of the models using the two respective data sets (measured and predicted inside conditions, Table 2 row IV) clearly shows the preference of PMsc over PMin by all statistical measures.

Discussion

The sensitivity analysis shows the change in evapotranspiration due to variations in the major meteorological variables. In this analysis each meteorological parameter was varied independently of the other parameters, except for the dependence of VPD on temperature.

Figure 7 shows the relative variations in ET estimated by the PMin and PMsc models, respectively, due to changes in the four major meteorological variables. As anticipated from the model equation (Eq. 2), ET increases linearly with R_N and VPD and non-linearly with wind speed and air temperature. Both models showed highest sensitivity to R_N, then (in descending order) to temperature, VPD and wind speed, in agreement with the results of Möller et al. (2004) for an insect-proof screenhouse in which pepper was grown.

Figure 8 shows the sensitivity coefficients (i.e., derivatives of the curves in Fig. 7) as a function of each meteorological variable. It is first observed that, for both models, sensitivity decreases with increasing temperature and wind speed. One of the major effects of the screens is in reducing the wind speed near the canopy (Fig. 4d). The lower sensitivity at high wind speeds suggests that, under such climatic conditions, changing the screen properties (e.g., hole dimensions, thread thickness), which may affect wind speed inside the screenhouse, is less significant in changing ET than in regions of lower wind speeds. A similar conclusion can be drawn regarding temperature modifications under

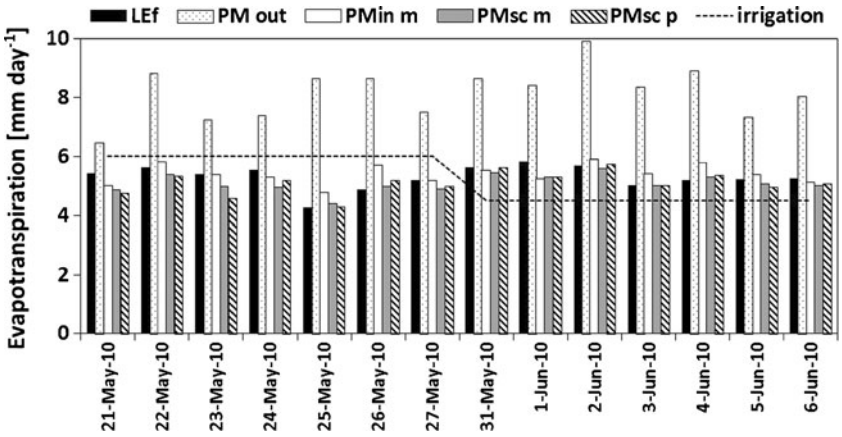

Fig. 6 Daily evapotranspiration (ET) during 14-day verification period: *black bars* LE_f; *dotted bars* PM outside (PM_{out}), *white bars* PM inside (PM_{in},); *grey bars* PMsc based on measured data, *hatched bars* PMsc based on predicted data, *horizontal dashed line*; irrigation. 21 May–6 June 2010

screens: in warmer regions changes in temperature will have a smaller effect on ET than in cooler regions.

Another observation from Fig. 8 is that PMsc is more sensitive to changes in net radiation than PMin; however, PMin is more sensitive than PMsc to variations in temperature, VPD and wind speed. Higher sensitivity of a model suggests that small errors in the measurements of the meteorological variables may cause larger errors in the ET prediction. Hence, the PMsc model would be more susceptible to errors in R_N than PMin, whereas the PMin model would be more susceptible than PMsc to errors in the components of the aerodynamic term.

Figure 9 illustrates the relative variation of ET estimated with PMin and PMsc models at different wind speeds. The limited distribution of the different wind speed curves observed for the PMsc model indicates its lower susceptibility to changes in wind speed compared to the PMin model, as was also indicated in Fig. 8d. It can be seen from Fig. 9a that, at higher VPD, the PMin sensitivity to changes in wind speed increases (as represented by the larger vertical intervals between the wind speed curves). This finding agrees with Allen et al. (1998) who showed that, in drier regions (larger VPD), changes in the wind speed have a greater impact on ET than in more humid regions (lower VPD). This behavior is also illustrated by the dashed line in Fig. 8d, which shows that the PMin sensitivity coefficient to wind speed is greater for larger VPD. Therefore, in moist areas, using screens and/or modifying screens features to reduce wind speed will be less effective for reduction in ET than in drier regions.

Table 2 Mean daily ratio between evapotranspiration (ET; mm day^{-1}) estimated by each model using measured data ($model_m$) inside the screenhouse and measured ET represented by LE_f, for the calibration (I) and verification (II) periods. Row III shows the same ratio using predicted inside data ($model_p$). Row IV shows the ratio between results yielded by each model calculated with predicted and measured data, i.e., the ratio between rows III and II. *STDEV* Standard deviation, *RMSE* root mean square error, *WI* Willmott's index of agreement (Willmott 1982), *NSE* Nash-Sutcliffe efficiency coefficient (Nash and Sutcliffe 1970)

ET models			PM_{in}	PMsc
Calibration 5 May–20 May	I	Avg $model_m/LE_f$	0.97	0.92
		(STDEV)	(0.06)	(0.04)
		RMSE [mm day^{-1}]	0.39	0.53
		WI [−]	0.88	0.79
		NSE [−]	0.61	0.30
Verification 21 May–6 June	II	Avg $model_m/LE_f$	1.02	0.96
		(STDEV)	(0.08)	(0.05)
		RMSE [mm day^{-1}]	0.39	0.32
		WI [−]	0.63	0.74
		NSE [−]	−0.05	0.30
	III	Avg $model_p/LE_f$	0.96	0.96
		(STDEV)	(0.08)	(0.06)
		RMSE [mm day^{-1}]	0.42	0.37
		WI [−]	0.79	0.73
		NSE [−]	−0.16	0.10
	IV	Avg $model_p/model_m$	0.94	1.00
		(STDEV)	(0.11)	(0.03)
		RMSE [mm day^{-1}]	0.61	0.16
		WI [−]	0.98	1.00
		NSE [−]	−2.69	0.70

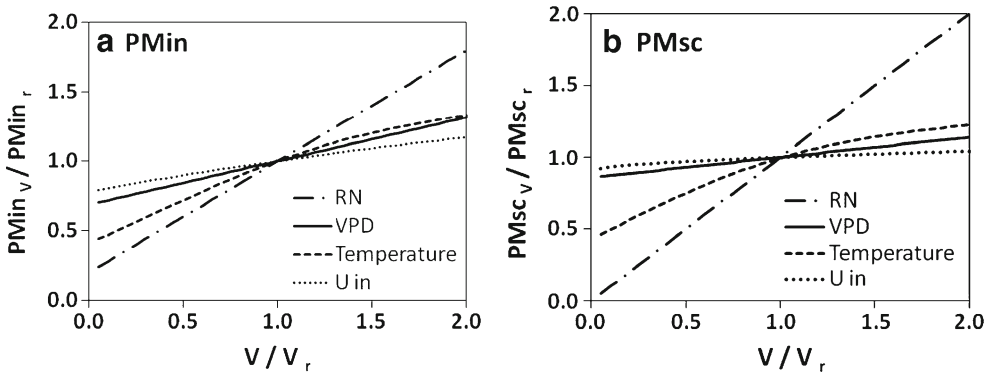

Fig. 7 Sensitivity analysis for **a** PMin and **b** PMsc to R_N (*dashed-dotted line*), VPD (*solid line*), temperature (*dashed line*) and wind speed (*dotted line*) at 1300 hours

Figure 9a shows a reversal point at VPD/VPD$_r \cong 0.3$. For VPD larger than this value, ET increases with wind speed, as expected; however, for VPD lower than this value increasing the wind speed would reduce ET. Monteith and Unsworth (1990) noted that this non-intuitive situation might happen when $LE/H < \Delta/(n\gamma)$, where $n=1$ for amphystomatal leaves and $n=2$ for hypostomatal leaves. Under these conditions, amplification of wind speed will increase H at the expense of LE, and therefore reduce LE. In the present analysis it was found that amplification of wind speed will increase ET ($S_u>0$) when $LE_{(PMin)}/H_{residual}>2.2$, whereas for $LE_{(PMin)}/H_{residual}<2.2$ amplification of wind speed will decrease ET ($S_u<0$). This result is shown graphically in Fig. 10. The critical value, $\Delta/n\gamma$, calculated for the current experiment (at 1300 hours and with $n=2$, appropriate to grapevine hypostomatal leaves) was 2.33, close to the value of $LE_{(PMin)}/H_{residual}$ at the point where S_u changes sign, as indicated in Fig. 10. In the present study, conditions of $LE_{(PMin)}/H_{residual}<2.2$ occurred during the morning hours when VPD≤0.4 kPa. These observations suggest that , under such climatic conditions, using screens for wind protection will not necessarily reduce water consumption and may even increase it.

Figure 9b and e show the variation in ET due to changes in temperature at different wind speeds, whereas VPD varied due to its dependence on temperature. Since the increase in temperature involves an increase in VPD, the effect on ET of temperature changes in different wind speeds would be qualitatively similar to that observed in Fig. 9a and d. For example, for the PMin model: in very hot regions—corresponding to a temperature increase of 20 % (to 43 °C)—VPD rises by 43 %. Under such conditions, increasing the wind speed twice or by four times (i.e., from 0.42 m s^{-1} to 0.84 m s^{-1} and to 1.68 m s^{-1}) will raise ET by 22 % and 65 %, respectively (from

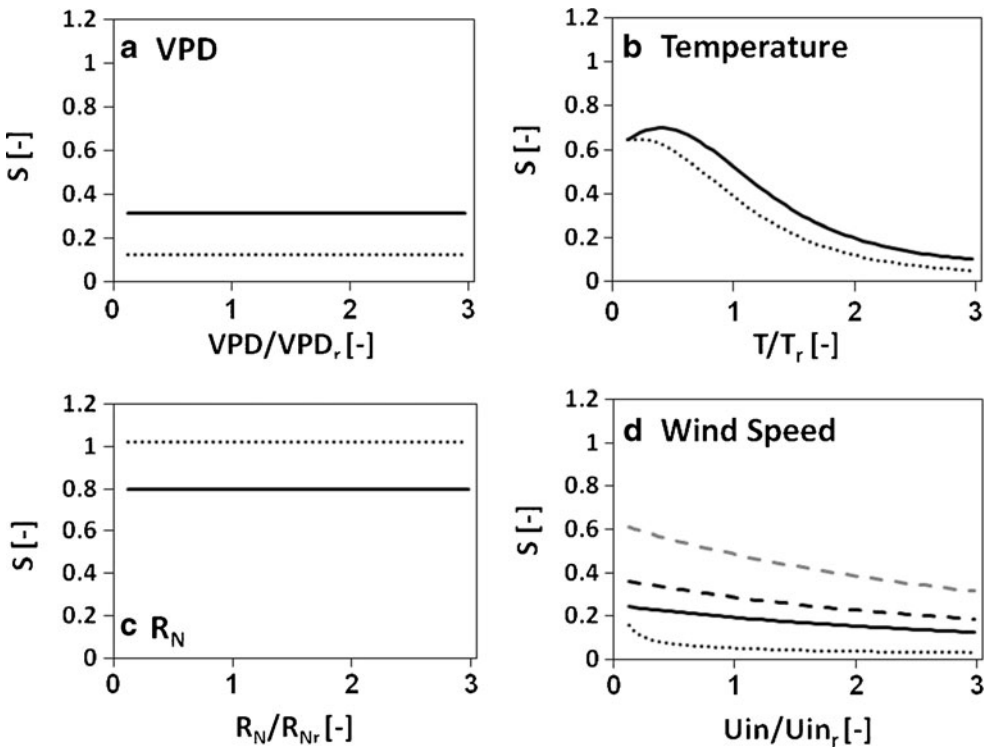

Fig. 8 Sensitivity coefficients for PMin (*solid line*) and PMsc (*dotted line*) to **a** VPD, **b** temperature, **c** R_N and **d** wind speed. The analysis was performed at 1300 hours with reference values: PMin$_r$= 457 W m^{-2}; PMsc$_r$= 391 W m^{-2}; VPD$_r$=4.09 kPa; T_r=36 °C; $R_{N\,r}$=506 W m^{-2}; $u_{in\,r}$=0.42 m s^{-1}. Panel **d** also shows the sensitivity coefficient of wind speed for PMin when $R_N=0.4R_{Nr}$ (*gray dashed line*) and VPD=1.5VPDr (*black dashed line*)

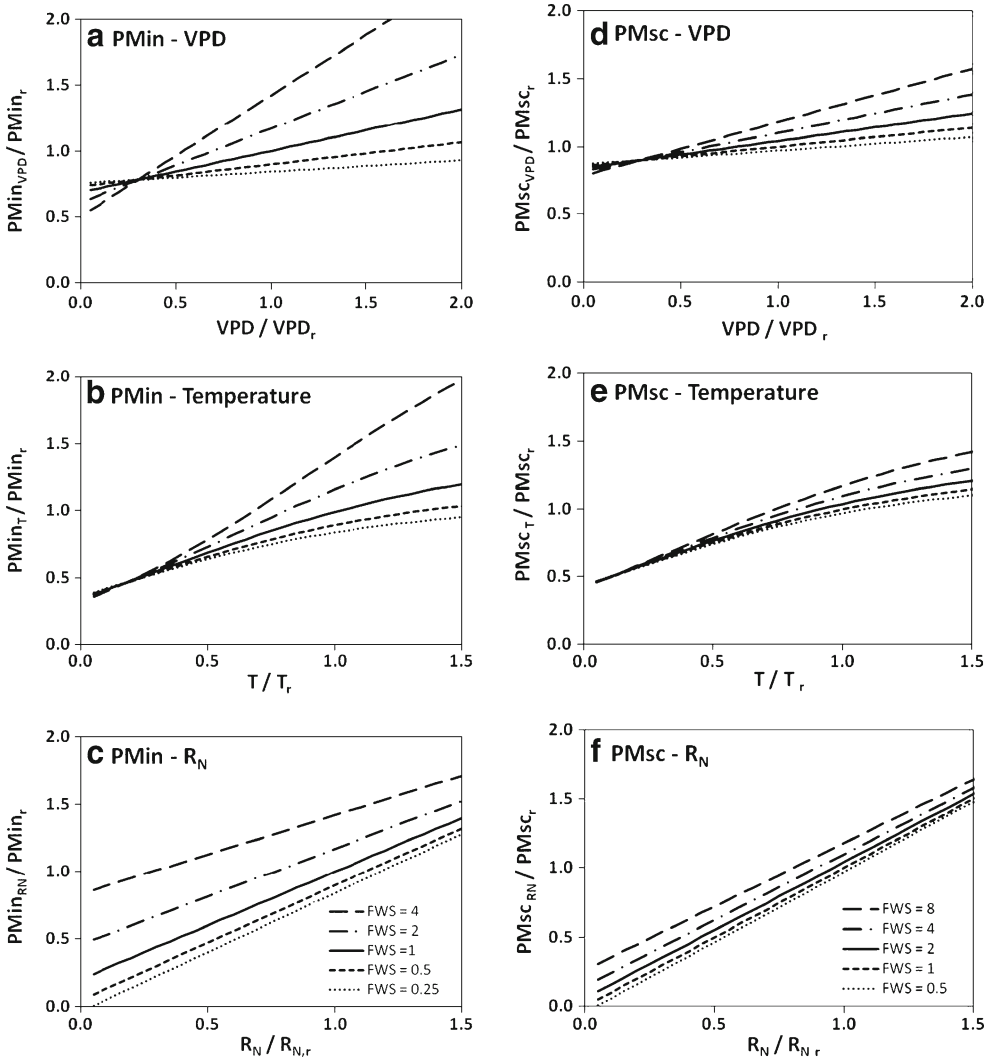

Fig. 9 Sensitivity analysis to **a**, **d** VPD; **b**, **e** temperature; and **c**, **f** R_N, for PMin (*left graphs*) and PMsc (*right graphs*), respectively, at different internal wind speeds. The analysis was performed for reference values (at 1300 hours): $PMin_r$= 457 W m^{-2}; $PMsc_r$=391 W m^{-2}; VPD_r=4.09 KPa; T_r=36 °C; $R_{N\,r}$ =506 W m^{-2}; $u_{in\,r}$=0.42 m s^{-1}

494 W m^{-2} to 594 W m^{-2} and 750 W m^{-2}). However, in cooler regions—corresponding by decreasing the temperature by 50 % (to 18 °C)—VPD will be reduced by 66 %, and the same two- and four-fold increases in wind speed will raise ET by only 5 % and 10 %, respectively (from 311 W m^{-2} to 334 W m^{-2} and to 357 W m^{-2}).

Figure 9c and f show the effect of changes in net radiation on ET at different wind speeds. As expected, as wind speed increases, ET increases, but as R_N increases, wind speed changes have less effect on ET. This is because, at high net radiation, the contribution of the radiative term in the PM equation (Eq. 2) increases at the expense of the aerodynamic term. This behavior is illustrated, for example, in Fig. 8d where the gray dashed line shows that the PMin sensitivity coefficient to wind speed is greater for lower R_N. The implication of this finding is that, for higher net radiation conditions, small changes in screen properties (such as screen texture or size of holes), which may also affect the wind speed under the screen, will have less influence on ET than the effect of the same changes in the screen under conditions of lower net radiation.

The present study has two significant implications. First, it shows the potential reduction in crop water use within the screenhouse as compared with cultivation of a similar crop outside, which highlights the need to develop models that accurately predict the crop water requirement: inaccurate irrigation, and especially excessive irrigation, may cause waterlogging, root damage and water losses below the root zone. Secondly,

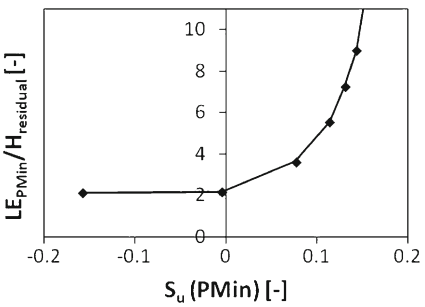

Fig. 10 Mean daily curve of positive values of *LE*/*H* (*LE* estimated by PMin model; *H* calculated as residual from energy balance components) as a function of the sensitivity coefficient to wind speed (S_u)

this study confirms the capability of the suggested modeling approach of using standard external meteorological data—easily obtainable by growers–to predict ET inside screenhouses, and thereby to improve their irrigation management.

However, calibration of internal data on the basis of external meteorological measurements is specific with respect to crop, screenhouse type, agro-technology and climate. The sensitivity analysis presented here can somewhat compensate for this limitation. It allows one to run a short-term calibration campaign and then use the model for different weather conditions or screens with different properties. Thus, it is envisaged that, for a certain crop grown under the same agro-technology, a calibration campaign like the one presented here would be worthwhile, followed by a corresponding sensitivity analysis for a more general application. It would provide growers with a tool for reliable ET estimation that would assist in irrigation decision making.

Major conclusions

1. The screenhouse can potentially reduce ET by 34 % on average, which highlights the importance of developing an accurate tool to estimate crop water requirements under screens.
2. Applying the models with predicted inside data, obtained from calibration against measured outside data, resulted in ET predictions that deviated by up to 6 % from model predictions based on the measured internal data.
3. Both models predicted internal ET within 8 %. Statistical analysis did not indicate a preference for any of the models.
4. All inside parameters necessary for the ET models were well represented by outside standard meteorological data, with statistically significant regressions.
5. The sensitivity analysis demonstrated the anticipated changes in ET due to changes in certain meteorological variables and screen properties. This tool is useful for the application of the models under operational conditions different from those presented here.

Acknowledgments The authors acknowledge technical support by A. Grava and M. Bahar. The present study was supported by the Chief Scientist of the Israeli Ministry of Agriculture and Rural Development, under grant number 304-0394. The research was also supported by Research Grant Award No. IS-4374-11C from BARD, the United States–Israel Binational Agricultural Research and Development Fund.

References

Allen RG, Pereira LS, Raes DM (1998) Crop evapotranspiration, guidelines for computing crop water requirements. FAO Irrigation and Drainage Paper 56, FAO, Rome, Italy

Campbell Scientific Inc (1998) Eddy covariance system–operator's manual, CA27 and KH20. Campbell Scientific, Logan, UT

Cohen S, Raveh E, Li Y, Grava A, Goldschmidt EE (2005) Physiological responses of leaves, tree growth and fruit yield of grapefruit trees under reflective shade screens. Sci Hortic 107:25–35

Desmarais G, Ratti C, Raghavan GSV (1999) Heat transfer modeling of screenhouses. Sol Energy 65:271–284

Dicken U, Cohen S, Tanny J (2012) Effect of plant development on turbulent fluxes of a screenhouse banana plantation. Irrig Sci. doi:10.1007/s00271-012-0346-0

Foken T, Gockede M, Mauder M, Mahrt L, Amiro B, Munger W (2004) Post-field data quality control. In: Lee X, Massman W, Law B (eds) Handbook of micrometeorology—a guide for surface flux measurement and analysis. Kluwer, Dordrecht

Franssen HJH, Stockli R, Lehner I, Rotenberg E, Seneviratne SI (2010) Energy balance closure of eddy-covariance data: a multisite analysis for European FLUXNET stations. Agric For Meteorol 150(12):1553–1567

Grace J (1980) Boundary layer conductance of the leaves of some tropical timber trees. Plant Cell Environ 3:443–450

Holman JP (1989) Heat transfer. McGraw-Hill, Singapore

Hsieh CI, Katul GG, Chi TW (2000) An approximate analytical model for footprint estimation of scalar fluxes in thermally stratified atmospheric flows. Adv Water Resour 23:765–772

Kittas C, Katsoulas N, Rigakis N, Bartzanas T, Kitta E (2012) Effects on microclimate, crop production and quality of a tomato crop grown under shade nets. J Hortic Sci Biotechnol 87(1):7–12

Kowalski AS, Anthoni PM, Vong RJ, Delany AC, Maclean GD (1996) Deployment and evaluation of a system for ground-based measurement of cloud liquid water turbulent fluxes. J Atmos Ocean Technol 14:468–479

Möller M, Tanny J, Li Y, Cohen S (2004) Measuring and predicting evapotranspiration in an insect-proof screenhouse. Agric For Meteorol 127:35–51

Möller M, Cohen S, Pirkner M, Israeli Y, Tanny J (2010) Transmission of short-wave radiation by agricultural screens. Biosyst Eng 107(4):317–327

Monteith JL, Unsworth MH (1990) Principles of environmental physics. Arnold, London

Moore CJ (1986) Frequency response corrections for eddy correlation systems. Bound-Layer Meteorol 37:17–36

Moratiel R, Martinez-Cob A (2012) Evapotranspiration of grapevine trained to a gable trellis system under netting and black plastic mulching. Irrig Sci 30:167–178

Nash JE, Sutcliffe JV (1970) River flow forecasting through conceptual models: part I—a discussion of principles. J Hydrol 10:282–290

Rana G, Katerji N, Introna M, Hammami A (2004) Microclimate and plant water relationship of the "overhead" table grape vineyard managed with three different covering techniques. Sci Hortic 102:105–120

Raveh E, Cohen S, Raz T, Yakir D, Grava A, Goldschmidt EE (2003) Increased growth of young citrus trees under reduced radiation load in a semi-arid climate. J Exp Bot 54:365–373

Rossel H, Ferguson J (1979) A new and economical screenhouse for virus research in tropical areas. FAO Plant Prot Bull 27:74–76

Schmid HP (1997) Experimental design for flux measurements: matching the scales of observations and fluxes. Agric For Meteorol 87:179–200

Siqueira M, Katul G, Tanny J (2012) The effect of the screen on the mass, momentum, and energy exchange rates of a uniform crop situated in an extensive screenhouse. Bound-Layer Meteorol 142:339–363. doi:10.1007/s10546-011-9682-5

Stanhill G (1969) A simple instrument for the field measurement of turbulent diffusion flux. J Appl Meteorol 8:509–513

Tanny J, Cohen S (2003) The effect of a small shade net on the properties of wind and selected boundary layer parameters above and within a citrus orchard. Biosyst Eng 84:57–67

Tanny J, Cohen S, Teitel M (2003) Screenhouse microclimate and ventilation: an experimental study. Biosyst Eng 84:331–341

Tanny J, Haijun L, Cohen S (2006) Airflow characteristics, energy balance and eddy covariance measurements in a banana screenhouse. Agric For Meteorol 139:105–118

Tanny J, Cohen S, Grava A, Naor A, Lukyanov V (2009) The effect of shading screens on microclimate of apple orchards. Acta Horticult (ISHS) 807:103–108

Tanny J, Dicken U, Cohen S (2010) Vertical variations in turbulence statistics and energy balance in a banana screenhouse. Biosyst Eng 106:175–187

Teitel M, Wenger E (2010) The effect of screenhouse roof shape on the flow patterns—CFD simulations. Acta Horticult 927:603–610

Teitel M, Peiper UM, Zvieli Y (1996) Shading screens for frost protection. Agric For Meteorol 81:273–286

Twine TE, Kustas WP, Norman JM, Cook DR, Houser PR, Meyers TP, Prueger JH, Starks PJ, Wesely ML (2000) Correcting eddy covariance flux underestimates over a grassland. Agric For Meteorol 103:279–300

Webb EK, Pearman GI, Leuning R (1980) Correction of flux measurements for density effects due to heat and water vapour transfer. Q J R Meteorol Soc 106:85–100

Willmott CJ (1982) Some comments on the evaluation of model performance. Bull Am Meteorol Soc 63:1309–1313

Wilson K, Goldstein A, Falge E, Aubinet M, Baldocchi D, Berbigier P, Bernhofer C, Ceulemans R, Dolman H, Field C, Grelle A, Ibrom A, Law BE, Kowalski A, Meyers T, Moncrieff J, Monson R, Oechel W, Tenhunen J, Valentini R, Verma S (2002) Energy balance closure at FLUXNET sites. Agric For Meteorol 113:223–243